Article

Not peer-reviewed version

Erosion Behaviour of Co-28Cr and WC-12Co Coatings on SA213-T22 Boiler Steel

Aumpava Kiatisereekul , Thamrongsin Siripongsakul , Kittichai Fakpan *

Posted Date: 26 July 2023

doi: 10.20944/preprints202307.1675.v1

Keywords: High velocity oxy-fuel; WC-Co; Co-28Cr; microhardness; erosion; T22 steel

Article

Erosion Behaviour of Stellite-6 and WC-12Co Coatings on SA213-T22 Boiler Steel

Aumpava Kiatisereekul [1], Thamrongsin Siripongsakul [2] and Kittichai Fakpan [2,*]

[1] Department, Faculty of Engineering; King Mongkut's University of Technology North Bangkok, 10800, Thailand

[2] Department, Faculty of Engineering; King Mongkut's University of Technology North Bangkok, 10800, Thailand

* Correspondence: kittichai.f@eng.kmutnb.ac.th; Tel.: +662-5874335

Abstract: At Mae-Moh power plant, Thailand, superheater tubes, which are exposed in fly ash environment, often degrade due to solid particle erosion. To extend the service lifetime of the superheater tubes, the high velocity oxy-fuel (HVOF) thermal spray technique is used to deposit a protective coating on the material, SA213-T22 steel. In this work, the solid particle erosion of Stellite-6 and WC-12Co coatings was investigated using erodent particle impingement at the angles of 30° and 90°. This was done with an average particle size of 60 μm. The erosion behavior of SA213-T22 with and without Stellite-6 and WC-12Co coatings was explained using ductile and brittle erosion. The erosion testing resulted in the brittle mode for both Stellite-6 and WC-12Co coatings, while SA213-T22 without coating indicated the ductile mode. On the investigation of surface morphology, the SA213-T22 steel showed ploughing and microcutting. The Stellite-6 coating showed some ductile erosion such as lips, different from the WC-12Co coating which showed microcracks and deep cavities. Erosion resistance of the Stellite-6 coating was higher than the WC-12Co coating. This was due to the strength and toughness of the metal matrixed composite structure and the low porosity of the coating.

Keywords: high velocity oxy-fuel; WC-Co; Stellite-6; microhardness; erosion; T22 steel

1. Introduction

The power industry suffers from severe corrosion and erosion problems, resulting in substantial losses. Erosion results from the impact of particulates, such as coal ash, delomite and unburned carbon particles on the surface of heated boiler tubes [1]. As a general rule, solid particle erosion refers to the progressive loss of original material due to mechanical interaction between the substrate and the erodent particles carried by the flue gas [2–5]. The solid particle erosion mechanism and erosion rates depend on particle properties, substrate properties and impingement conditions. Several studies have discussed how particle hardness (H_P) and target hardness (H_t) affect erosion rate [6,7]. Solid particle erosion mechanisms can be divided into two major categories: ductile and brittle. Ductile erosion happens when the material is removed due to cutting and ploughing action, while brittle erosion is characterized by the formation of cracks and fractures on the material surface [8,9].The major difference between those two modes can be clarified when erosion rates differ due to different impingement angles. Ductile materials usually show more erosion rates at shallow impingement angles. On the other hand, erosion rates of the brittle are dominant at impingement angles close to the normal angle [10,11]. Recently, the thermal spray processes represent an important and cost effective technique for coating the surface of metals to enhance their durability and performance under a variety of operating conditions. The high velocity oxy-fuel (HVOF) technique is the thermal spray process which forces particles with high kinetic energy to be attached to the surface of the material. The deposited particles are generally in the plastic state, leading to obtain dense coating [12–14]. The HVOF spray technique has been expected as a viable coating technique

 doi:10.20944/preprints202307.1675.v1

for in-situ applications, wear and corrosion managements and dimensional restoration due to its high bonding strength, low porosity and low stress coatings. Kumar et al. reported that the 35% WC+NiCrBSiC coating showed a high level of quality in terms of hardness and low porosity [1,15]. The increase of the WC content from 0 to 35% significantly improved hardness of the coating without decreasing toughness. Carbide based coatings have been widely used in abrasive, erosive and oxidizing environments. It was reported that the carbide-based coatings exhibited high hardness with a high volume fraction of carbide and high wear resistance [16].

Cobalt has been reported that it is one of the important elements affecting the hardness and toughness of the materials. Cobalt alloy coatings are exceptionally good for applications requiring resistance to corrosion, erosion, cavitation and wear. For example, WC-Co coatings are often used in applications requiring abrasive wear resistance [1,17,18]. When cobalt is added to tungsten carbide, it improves adhesion and wettability [19].

In order to improve the service life of power plant boiler steel SA213-T22, Stellite-6 and WC-12Co coatings were applied to the materials and a comparison of erosion was performed. In addition, to clarify the quality of the hard coatings in a short period of time, slicon carbide, which was one of the hardest materials, was used as erodent particle.

2. Experimental

2.1. Materials and Coating Process

SA213-T22 boiler steel was obtained from the Mae Moh power plant in Lampang province, Thailand. The steel was in a tube shape with a diameter of 50.8 mm and thickness of 9.1 mm. The chemical composition (wt%) analysed by a standard emission spectroscopy technique is shown in Table 1.

Table 1. Chemical compositions of SA213-T22 steel [20].

Composition (wt. %)	C	Mn	Si	S	P	Cr	Mo	Fe
T22 steel	0.11	0.43	0.27	0.011	0.016	1.93	0.92	Bal.
ASTM SA213-T22	0.15	0.3-0.6	0.5	0.03	0.03	1.9-2.6	0.87-1.13	Bal.

Stellite-6 and WC-12Co powders with particle size of 15–45 μm were used in the HVOF process. The powders and process were supported by Hummingbird Corporation Co., Ltd., Thailand. The chemical compositions and particle sizes of the coating powders are shown in Table 2. The SA213-T22 steel substrates were prepared with dimensions of 15 mm x 15 mm x 3 mm prior to coating. And then they were cleaned with acetone and grit-blasted using an alumina abrasive powder. The coatings were deposited on SA213-T22 steel substrates using a HVOF coating machine, a Termika-3 system. Propane and oxygen were used as fuel and working gases, respectively. The process parameters for HVOF coating are shown in Table 3. The parameters were optimized by Hummingbird Corporation Co., Ltd.

Table 2. Compositions for HVOF coating powders [21].

Coating Powder	Average Particle Size (μm)	Composition (Weight %)				
		C	Si	Cr	Co	W
Stellite-6	11-45 μm, Spherical	1	1	28	66	4
WC-12Co	15-45 m, Spherical	4	-	-	12	84

Preprints (www.preprints.org) | NOT PEER-REVIEWED | Posted: 26 July 2023 doi:10.20944/preprints202307.1675.v1

Table 3. Spray parameters employed for HVOF coating.

Parameters	Values
powder feed rate (g min^{-1})	25
Oxygen flow rate (O_2, l min^{-1})	50
Propane flow rate (C_3H_8, l min^{-1})	20
Air flow rate (l min^{-1})	400
Spray distance (mm)	200
Coating thickness (average, μm)	200
Maximal heat source temperature (^oC)	2,850

2.2. Erosion Experiments

Silicon carbide (SiC) was used as the erodent material, which is composed of crystalline SiC 98.10 %, Si 0.25 %, C 0.13 %, SiO_2 0.50 %, Fe_2O_3 0.12 % and other oxides 0.30 % by weight. According to the ASTM G76-05 standard, the accelerated solid particle erosion test was conducted at an ambient temperature using an air-jet type erosion tester as shown in Figure 1 [19]. The erosion tester consists of an air compressor pump, an erodent particle collector, a nozzle with a bore diameter of 6 mm and a sample holder. In cases where the particle was softer than the target ($H_p/H_t < 1$), the evaluation time was longer and very low erosion rates were observed [22–24,41,45]. SiC, one of the hardest materials, was used to clarify erosion rates in a short period of time [25–28]. The diameter of SiC used as an erodent particle is 60 μm. Its morphology is shown in Figure 1.

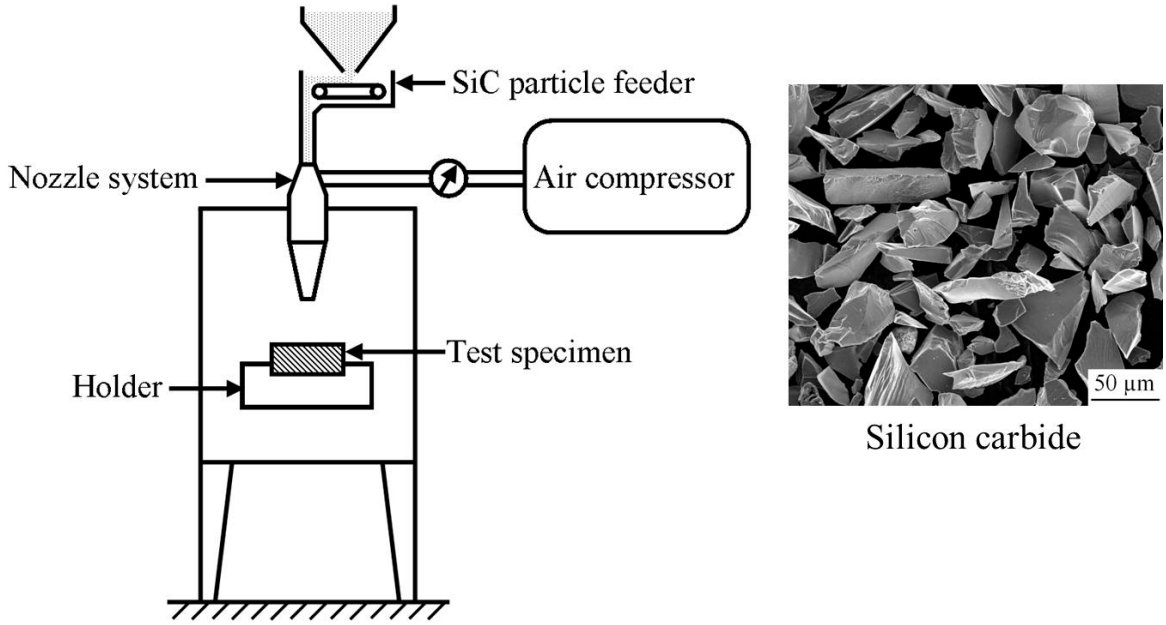

Figure 1. The schematic diagram of the air-jet type erosion tester and SEM micrograph of silicon carbide erodent particles.

The experimental parameters carried out are shown in Table 4. The average particle sizes of SiC erodent used in the tests was 60 μm in diameter and the feeding rate was 10 g·min^{-1} with a standoff distance of 20 mm The erodent particles were accelerated to pass through the nozzle; the particle velocities adjusted by the compressed air with a mass flow controller were 12.8, 22.5 and 38.9 m·s^{-1} for SiC sized 60 μm. The measurement of particle velocities was done by using a 1D laser Doppler anemometer. The calibration was supported by National Institute of Metrology, Thailand, and the result will be published elsewhere. The sample holder was able to be set at the impingement angles of 30^o and 90^o.

Preprints (www.preprints.org) | NOT PEER-REVIEWED | Posted: 26 July 2023 doi:10.20944/preprints202307.1675.v1

The erosion study was conducted on uncoated SA213-T22 and coated samples with parameters listed in Table 4. All of the coated samples were first ultrasonically cleaned in alcohol, dried and weighed to An analytical balance (Mettler Toledo) having the least count of 0.01 mg precision before testing. Prior to erosion testing, the uncoated samples were mechanically ground using abrasive papers up to 1,000 grits. While the coated samples were only cleaned ultrasonically in alcohol for 15 minutes before being dried. Mass loss was determined after samples were cleaned and dried after exposure to silicon carbide particles. An erosion rate (E) was calculated by dividing the sample mass change (Δm_t) to the particle mass (Δm_p) used in each test cycle with respect to ASTM standard. This was done according to the following equation [28,29]

$$E = \frac{\Delta m_t}{\Delta m_p} \quad (1)$$

Table 4. Parameters used for erosion testing.

Standoff distance (mm)	20
Test gas	Dry air
Test Duration (s)	60
Nozzle diameter (mm)	6
Test temperature	Room temperature
Particle velocity ($m \cdot s^{-1}$)	12.8, 22.5 and 38.9
Abrasive feed rate ($g\ min^{-1}$)	20
Angle of incidence (^{o})	30, 90
Air jet pressure (bar)	5

2.3. Characterisation

The surface morphology of the samples, both before and after the erosion test was observed using a field emission scanning electron microscope with energy dispersive spectroscopy (EDS) (FE-SEM/EDS) (Tescan, Mira3, Czech Republic) was used to determine the compounds in the coatings. The vickers test (HV-1000B) was carried out to measure the microhardness of the substrate and coatings. In addition, the surface roughness was also evaluated by a 3D laser microscope (Olympus OLS4000-SAF).

3. Results and Discussion

3.1. Characterisation

3.1.1. SEM/EDS and X-ray Diffraction Analysis

Figure 2a shows the surface morphology of the HVOF sprayed coating of Stellite-6 as deposited. The coating surface is continuous; a few un-melted particles with diameters ranging from 10 μm to 30 μm are also left. The coating presents a continuous surface but rough texture as a result of un-melted particles. The roughness of the coating was 13.5 μm evaluated by the 3D laser microscope. The cross-sectional micrograph of the coating is shown in Figure 2b. The coating has a small amount of porosity. Using Image J, the image analysis software, the average thickness of the coating is 215 ± 12 μm with an average porosity of 3.29 %. A line scanning element analysis in Figure 2c shows that the coating is consisted of Co and Cr. Oxygen in the coating is slightly increased compared to the steel substrate.

As shown in Figure 2d, the XRD pattern was derived from the top surface of Stellite-6 coating, indicating the composition of CoCr, WC and Cr_2O_3 phases. The Cr_2O_3 phase is not detected from Stellite-6 powder. According to the line scan and XRD results, oxidation occurred during high velocity oxy-fuel sprayed coating process was carried out, forming partially the protective Cr_2O_3 as deposited. The surface morphology of HVOF sprayed coating of WC-12Co is shown in Figure 3a. A

Preprints (www.preprints.org) | NOT PEER-REVIEWED | Posted: 26 July 2023 doi:10.20944/preprints202307.1675.v1

rough surface with small pores and un-melted particles is also observed. The roughness of the coating was 8.9 µm slightly lower than the Stellite-6 coating. The cross-sectional micrograph of the WC-12Co coating is shown in Figure 3b with the evaluated amount of porosity of 6.73%. The average thickness of the coating is 198 ± 7 µm. The line scanning element analysis of the coating is shown in Figure 3c exhibiting the presence of W, Co Cr and C, while oxide is less detected compared to the Stellite-6.

The XRD results of WC-12Co coating is shown in Figure 3d which indicates existence of WC and W_2C. The peaks of WC for 2θ values in 31.64°, 35.79°, 48.45°, 64.27°, 73.37°, 75.72°, 77.22°, 84.28° are obvious, indicating as the main phase of the coating. It is well known that in order to achieve an optimum wear property of the WC-M (M=Co, Ni, Cr, Mo) coating, the WC phase should be retained for a large volume fraction [16,30–32]. Whereas W_2C and Co are detected with quite low intensity, indicating less volume fractions of W_2C and metallic Co in the coating. Kreye investigated different phase transformations during HVOF spraying of two different WC-Co powders [33]. In casted and crushed type, WC, W_2C, Co_3W_3C and W existed in the coating. Substantial portion of the WC (about 30 to 50%) was transformed to W_2C and W. For agglomerated and sintered type of WC-Co powder, only WC and Co were detected. In the HVOF process performed in this study, only small portion of WC, less than 10%, was transformed to W_2C. The phases of W and Co_3W_3C were not detected in the coating.

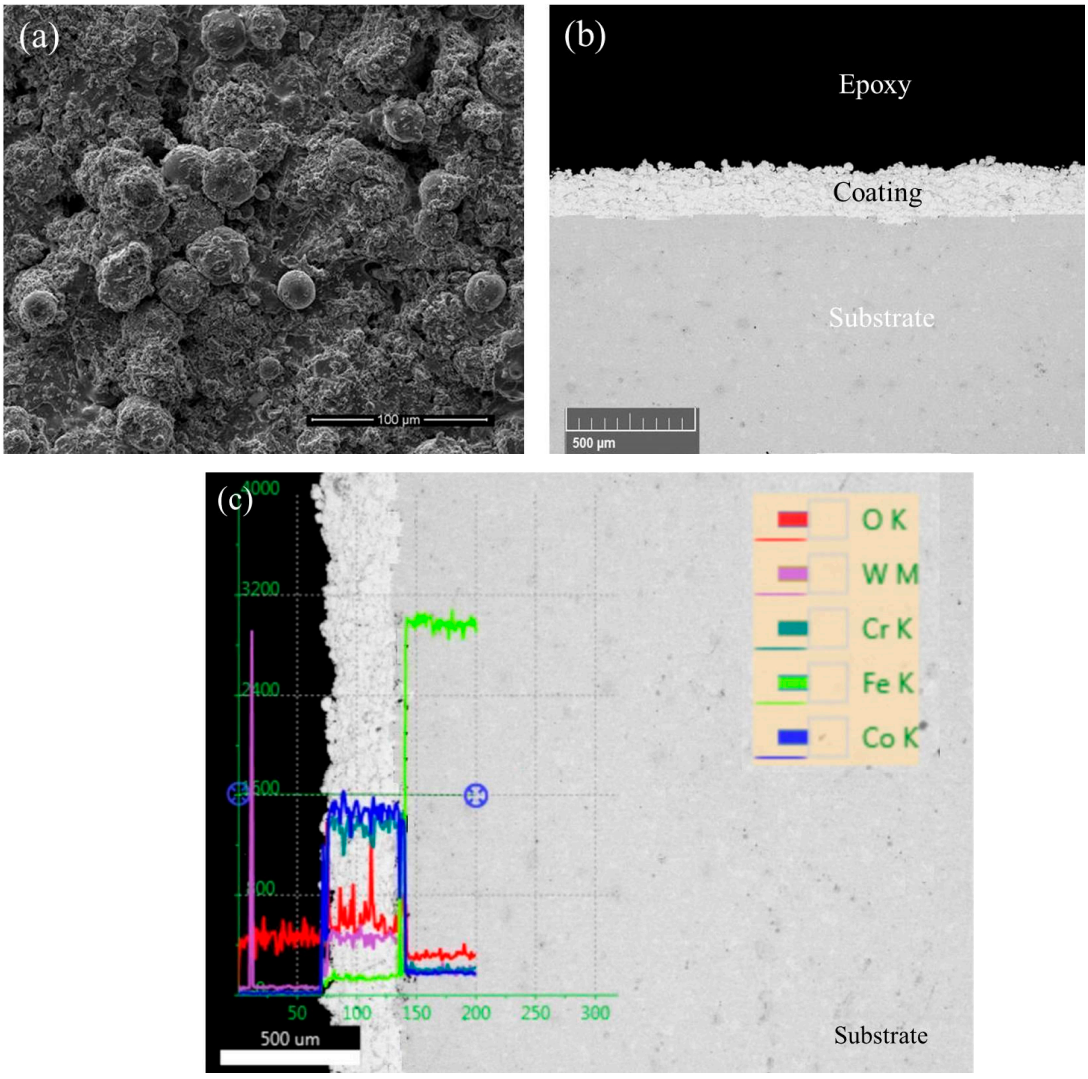

Preprints (www.preprints.org) | NOT PEER-REVIEWED | Posted: 26 July 2023 doi:10.20944/preprints202307.1675.v1

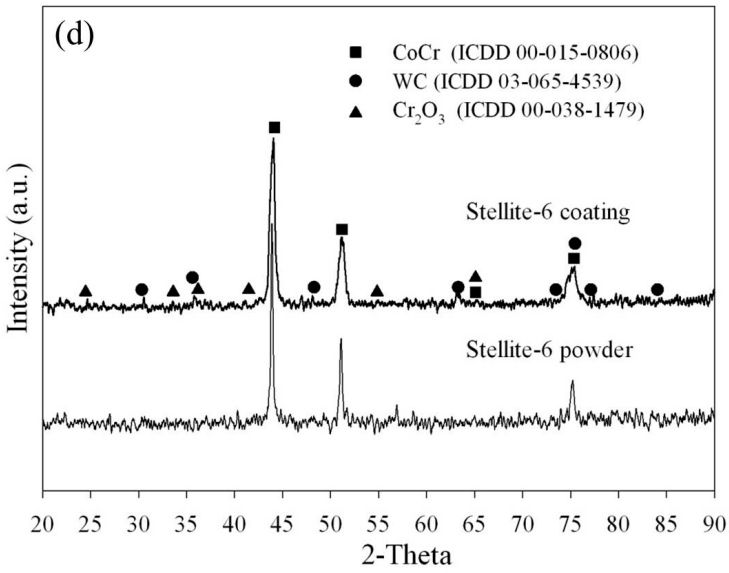

Figure 2. SEM micrographs (a) surface, (b) Cross sectional, (c) EDS line scan and (d) X-ray diffraction patterns of the high velocity oxy-fuel sprayed Stellite-6 coating.

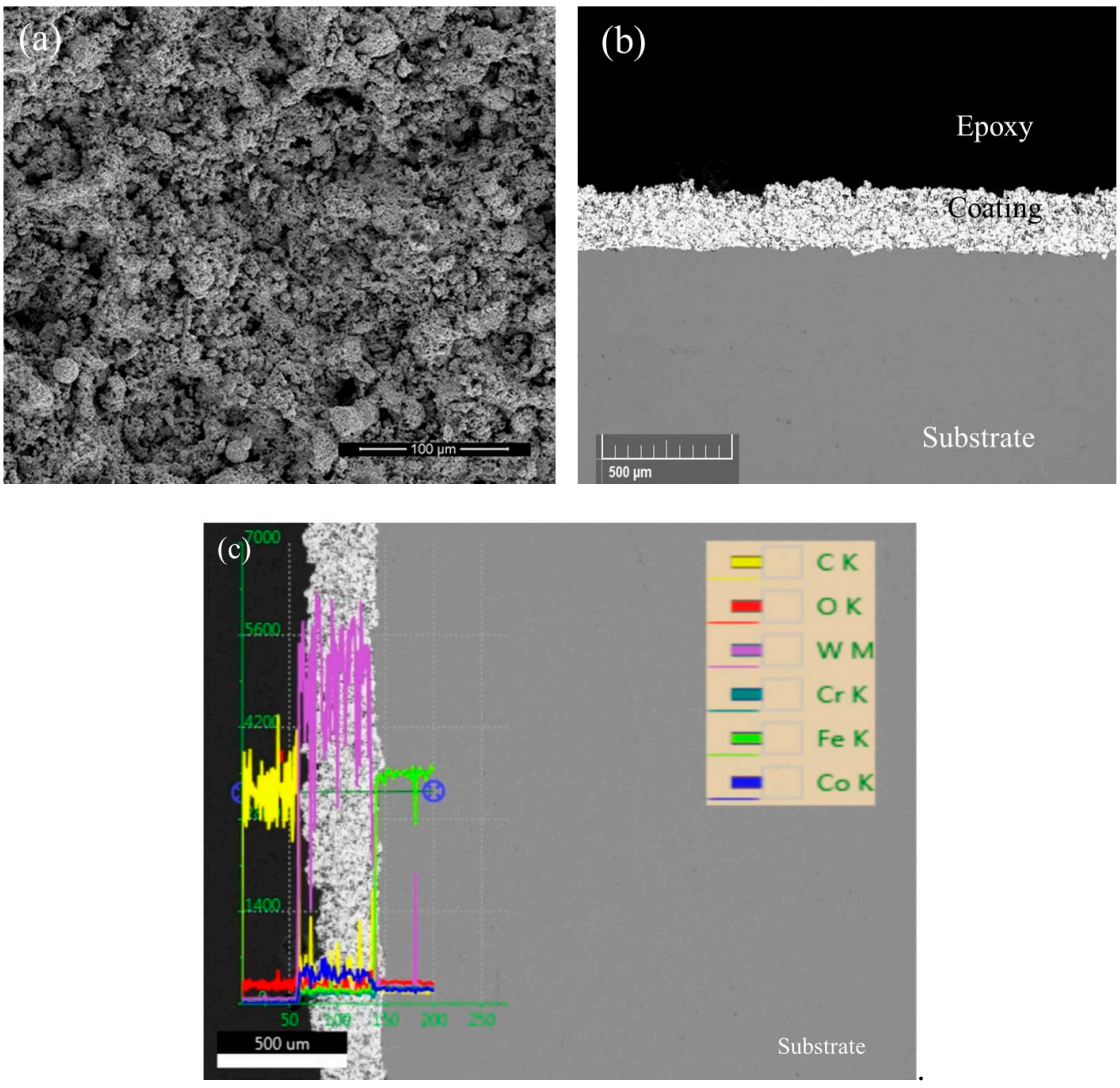

Preprints (www.preprints.org) | NOT PEER-REVIEWED | Posted: 26 July 2023 doi:10.20944/preprints202307.1675.v1

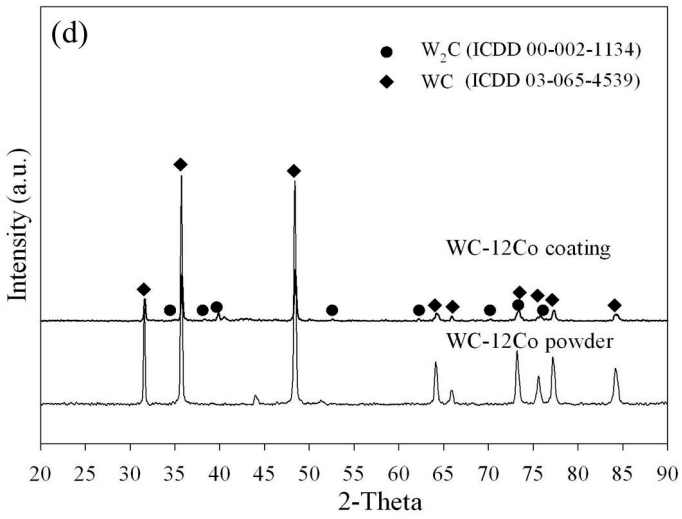

Figure 3. SEM micrographs (a) surface, (b) Cross sectional, (c) EDS line scan and (d) X-ray diffraction patterns of the high velocity oxy-fuel sprayed WC-12Co coating.

3.1.2. Hardness

The microhardness of the SA213-T22 substrate, Stellite-6 and WC-12Co coatings are shown in Figure 4. The average hardness value of uncoated sample was 143.97 Hv with discrepancy of 10 Hv, while the coatings produced by HVOF process yielded values of more than 500 Hv. The average hardness of WC-12Co coating was 745.67 Hv, whereas the one of Stellite-6 was 511.12 Hv. The hardness of Stellite-6 coating was comparable to the one of Stellite-6 coating reported by Mirsheka [34]. A WC-12Co coating on 316 stainless steel reported by Stack showed a hardness value of 616 Hv that is similar to this result [35]. However, with appropriate parameters and low porosity the hardness of this kind of coatings can reach approximately 1,300 (approximately 16GPa) [24,36,37]. The difference in hardness among research works could be attributed by decarburization, carbide grain size and density of the coating which are generated by various conditions in the HVOF process.

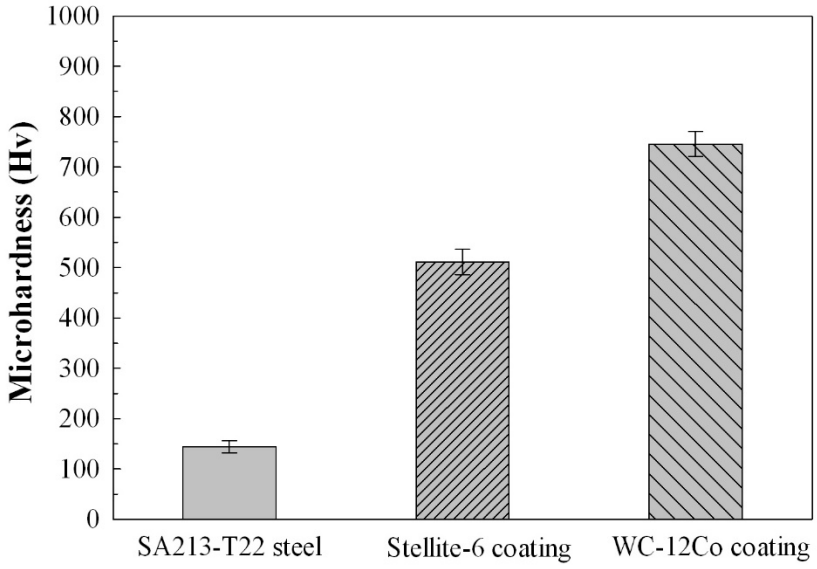

Figure 4. Microhardness of Stellite-6 and WC-12Co HVOF coating on SA213-T22 steel substrates.

3.2. Erosion Test

Preprints (www.preprints.org) | NOT PEER-REVIEWED | Posted: 26 July 2023 doi:10.20944/preprints202307.1675.v1

3.2.1. Erosion Rate and Velocity Exponent

Figure 5 shows steady erosion rates of SA213-T22 steel and the Stellite-6 and WC-12Co coated on SA213-T22 steel tested using of silicon carbide as erodent particle with impingement velocity of 12.8, 22.5 and 38.9 m·s^{-1}, and impingement angles of 30° and 90°. All of the erosion rates increased with an erodent particle velocity. For Stellite-6 and WC-12Co coatings, the erosion rates at the 90° were lower than those at 30°. Especially when the velocity was 12.8 m·s^{-1}, the ratios of erosion rates at 90° to those at 30° (E_{90}/E_{30}) of Stellite-6 and WC-12Co coatings were up to 1.58 and 1.30, respectively. The values of erosion rates as well as E_{90}/E_{30} of all samples were summarised in Table 5. Stellite-6 and WC-12Co coatings exhibited E_{90}/E_{30} values of more than 1, responding the erosion of the brittle mode. Conversely, the erosion rates of SA213-T22 steel, uncoated samples, exhibited the ductile mode with higher erosion rates at the 30° than those at 90°, thus the E_{90}/E_{30} values were less than 1. According to the erosion test results, Stellite-6 coating showed better wear tolerance than WC-12Co coating [38].

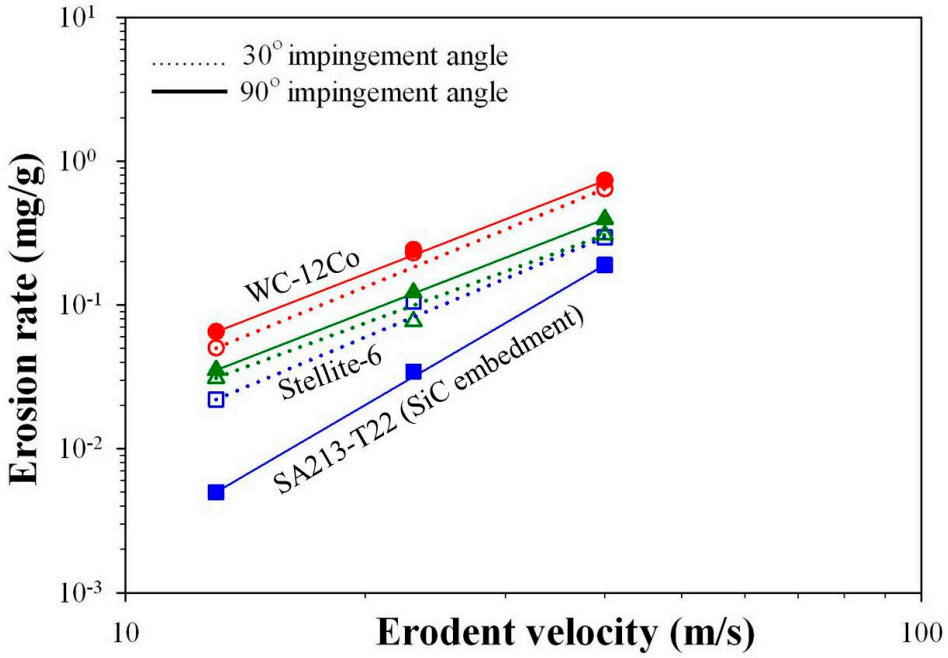

Figure 5. Erosion rates of SA213-T22 steel tested by various impingement velocities of erodent particle at impingement angles of 30°(open markers) and 90°(solid markers).

Principally an erosion rate is related to kinetic energy of erodent particles. Hardness, Young's modulus, mechanical properties, and surface morphology of erodent particles and substrates are also important factors leading to elastic and inelastic collision. Particle velocity is the most influential parameter affecting erosion. Empirically, the erosion rate at room temperature can be expressed by velocity exponent of the following equation; [6,24,28,29,39–41].

$$E = Kv^n \quad (2)$$

where E is the erosion or wastage rate, v is the impingement velocity, K is a material constant and n is a velocity exponent dependent on materials of erodent particles and substrates. The erosion rates were fitted well using equation (2) as shown in the Figure 5 by solid lines (90° impingement angle) and dotted lines (30° impingement angle) with the correlation coefficients of more than 0.91. The value of the velocity exponent is another parameter used to determine the ductile or brittle erosion. Such as for SA213-T22 steel which showed the ductile erosion behavior, the velocity exponent widely changed from 2.31 at 30° to 3.23 at 90° impingement angle. This drastic change indicated the sensitivity to erosion of the surface condition of the material [7]. The value at 30° was under Basu, who suggested that the velocity exponent value was 2.3-2.7 for ductile materials. While SiC embedment at 90° impingement caused the SA213-T22 surface to become a composite or brittle material, therefore the velocity exponent could exceed 3 [3,42]. For ductile erosion, erosion rates were

Preprints (www.preprints.org) | NOT PEER-REVIEWED | Posted: 26 July 2023 doi:10.20944/preprints202307.1675.v1

higher at 30° than at 90° impingement angle. A surplus amount of energy was required at 90° impingement angle for target deformation [24,29,38,43].

Thus higher velocity exponent responded to lower erosion rates than those at 30°. The values of velocity exponent are also summarized in Table 5. The velocity exponents of Stellite-6 and WC-12Co coatings were approximately 2; this followed the traditional rules using SiC as an erodent particle, as reported in other literature [3,27,42].

Table 5. Erosion rates, erosion ratio and velocity exponent of uncoated samples, Stellite-6 and WC-12Co coated samples.

Sample	Impingement Angle (°)	Erodent Particle Velocity (m/s)	Erosion Rate (mg/g)	Velocity Exponent (*n*)	E_{90}/E_{30}	Comment
SA213-T22	30	12.8	0.02			
		22.5	0.11	2.33		
		38.9	0.30			
	90	12.8	0.01		0.23	ductile
		22.5	0.03	3.27	0.33	ductile
		38.9	0.19		0.64	ductile
Stellite-6	30	12.8	0.03			
		22.5	0.08	2.06		
		38.9	0.31			
	90	12.8	0.04		1.14	brittle
		22.5	0.12	2.15	1.58	brittle
		38.9	0.40		1.29	brittle
WC-12Co	30	12.8	0.05			
		22.5	0.23	2.18		
		38.9	0.64			
	90	12.8	0.07		1.30	brittle
		22.5	0.24	2.30	1.06	brittle
		38.9	0.73		1.14	brittle

When the erodent particle velocity was 38.9 m/s, the erosion rates of uncoated SA213-T22 substrates were 0.2–0.3 mg/g, and those of samples with Stellite-6 and WC-12Co coatings were approximately 0.4 and 2.0 mg/g, respectively. The result of uncoated samples was comparable to the erosion rates of steels reported by Sapate, when alumina was used as erodent particle [43]. In comparison to Singh's report, coated samples had a slightly higher erosion rate [14]. SiC erodent particles have a stronger hardness of 2,481 Hv than alumina particles, resulting in the difference [24]. In addition to the above factors, the porosity, density, and chemical composition of coated samples also play a role in erosion behavior.

3.2.2. Surface Morphology and Chemical Composition Analysis

To understand the erosion behaviour, the surface of the sample after the erosion test was investigated using FE-SEM with EDX. The SEM micrographs with EDX analysis results of uncoated SA213-T22 steel, the Stellite-6 and WC-12Co coated samples after the erosion tests at 30° and 90° impingement angles are shown in Figures 6–8.

The EDX analysis of eroded SA213-T22 surface at 30° and 90° impingement angles is shown in Figure 6a,b. The detected chemical composition of Fe, Cr, Mo, C, Mn, S, P and Si is in conformance with the SA213-T22 steel. The presence of Si along with C clearly indicates that the erodent (SiC) has incrusted the substrate, as the Si to C ratios by mole after the erosion tests at 30° and 90° impingement angles were 1:1.12 and 1:0.98, respectively. The same result was reported for SiC embedding [1]. Thus, the embedment of SiC on the steel surface misled to low erosion rates of the aforementioned results.

Preprints (www.preprints.org) | NOT PEER-REVIEWED | Posted: 26 July 2023 doi:10.20944/preprints202307.1675.v1

However, the velocity exponent was quite sensitive to this phenomenon, and showed high sensitivity to erosion of SA213-T22. Inclusion of SiC mass after erosion tests at 90° was twice more than that at 30°. This was also the reason for the low erosion rate at normal angle of ductile materials.

The surfaces of Stellite-6 coating tested under impingement angles of 30° and 90° are shown in Figure 7a,b, respectively. The composition indicated Co, Cr, W, Fe and small amount of oxide. On the other hand, W, C, Co, Cr, Fe and O were detected in WC-12Co coatings as shown in Figure 8a,b. According to both EDX results, no detection of Si, thus SiC embedment did not occur on samples with Stellite-6 and WC-12Co coatings.

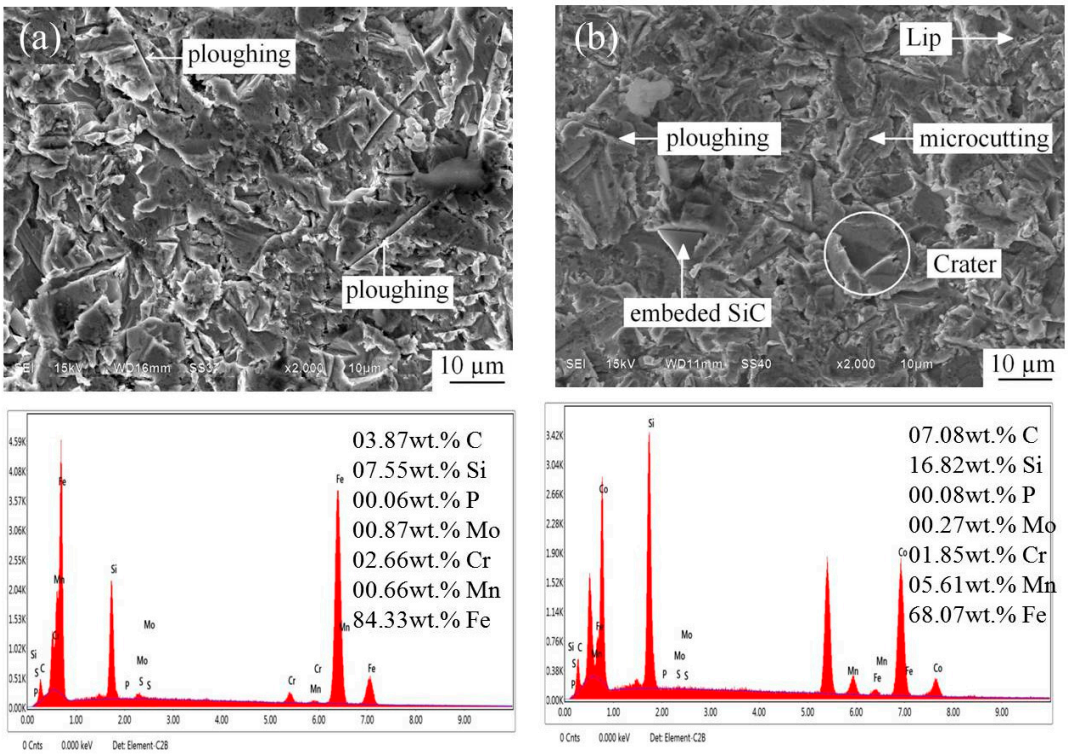

Figure 6. SEM images (upper) and EDX (lower) analysis result of SA213-T22 steel after the erosion test at velocity of 22.5 m/s at impingement angle a) 30° b) 90°.

Preprints (www.preprints.org) | NOT PEER-REVIEWED | Posted: 26 July 2023 doi:10.20944/preprints202307.1675.v1

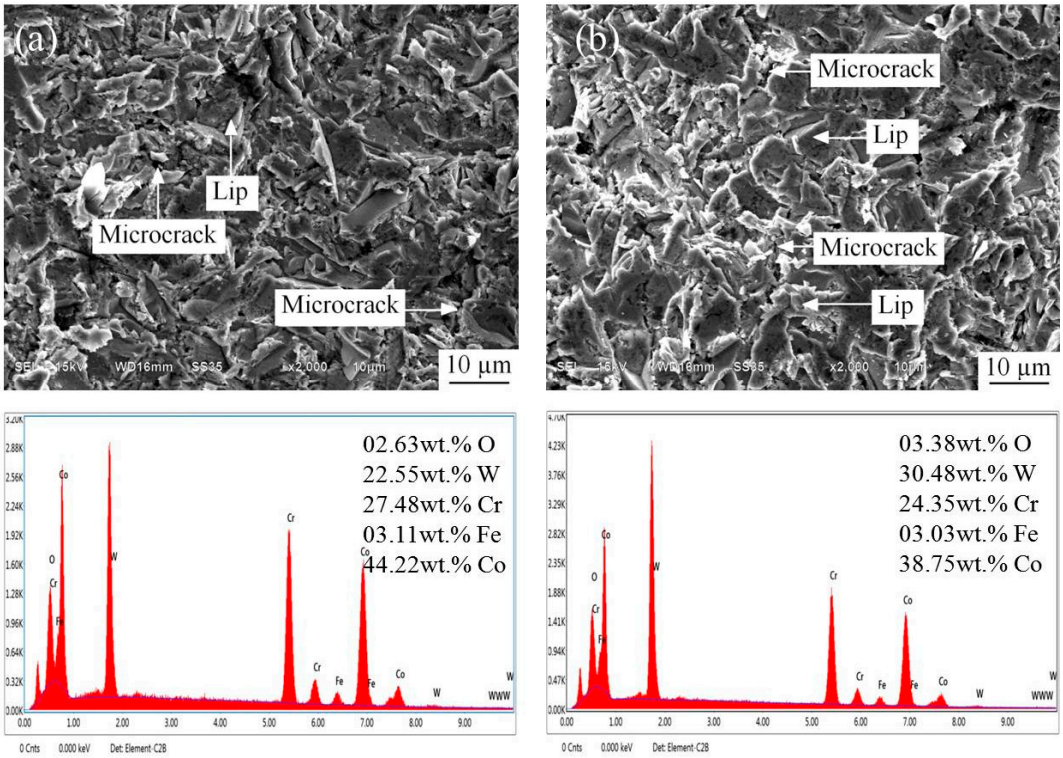

Figure 7. SEM/EDAX image of Stellite-6 at velocity of 22.5 m/s at impingement angle a) 30° b)90°.

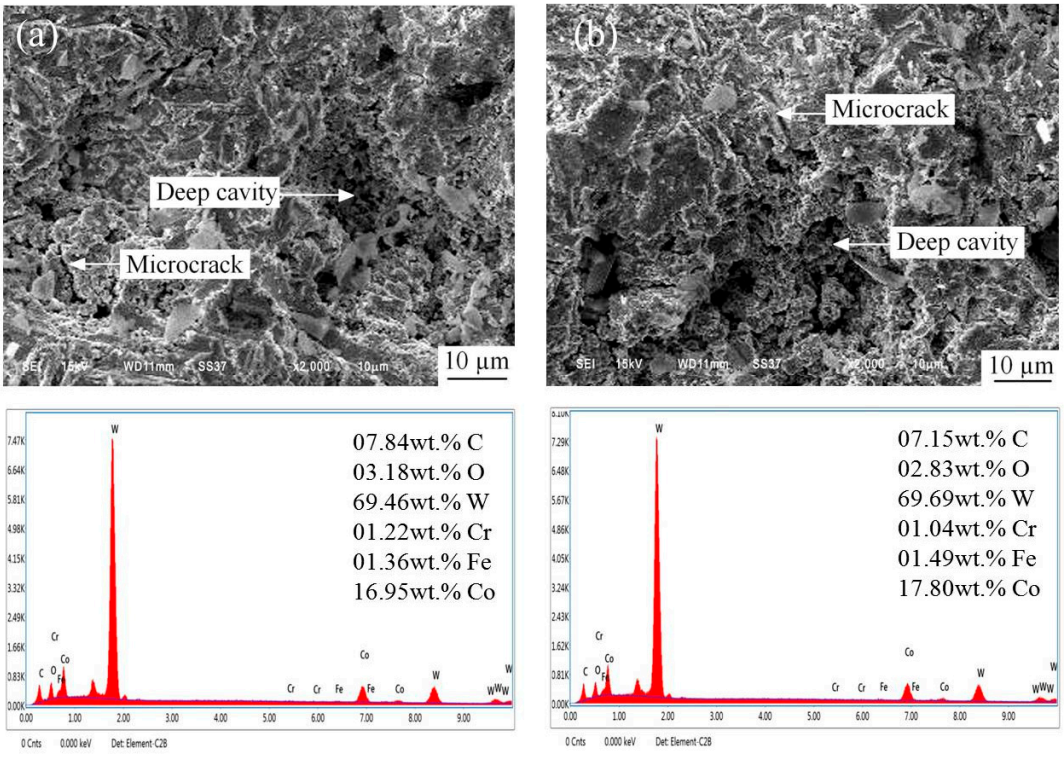

Figure 8. SEM/EDAX image of WC-12Co at velocity of 22.5 m/s at impingement angle a) 30° b)90°.

In general, the erosion characteristics of ductile materials at shallow impingement angles are dominated by ploughing, crater, cutting and shear deformation. Meanwhile at the normal impingement angle, low cycle fatigue and localization of plastic flow can occur. As is well known, erosion mechanisms are controlled by the ratio of erodent particle hardness (H_P) to target hardness

 doi:10.20944/preprints202307.1675.v1

(H_t). The ratio of erodent particle hardness to target surface hardness (H_p/H_t) is to be considered for evaluating coating erosion behavior. Experimental results indicated that abrasive particles would cause plastic scratching and indent the surface, only if H_p/H_t was more than 1.2 [1,6,44]. In cases where the particle was softer than the target (H_p/H_t is less than 1), very low erosion rates were observed [45]. In the case of SA213-T22 steel, the H_p/H_t ratio of 17.23 indicated ductile erosion with plastic deformation resulting in SiC particles penetration into the substrate surface. The SEM image in Figure 6a shows the morphology after the erosion test at 30°. Tracks of ploughing lines can be clearly found. The surface after the 90° test in Figure 6b shows microcutting, and embedded SiC. Sequentially, shielding affects against erodent particles due to embedment of hard SiC can lead to apparently low erosion rates. The impingement at an angle at 30° results in more ploughing lines but less SiC embedment.

On the impingement surface of Stellite-6 and WC-12Co coatings, erosion behaviour played a role in crack nucleation and propagation. Figure 7a,b show microcracks and lips within the Stellite-6 coating. In spite of the fact that the E_{90}/E_{30} ratio was greater than 1, ductile erosion was also observed on the Stellite-6 coating. As the H_p/H_t ratio of Stellite-6 coating was 4.85 Hv, this indicated that plastic deformation such as libs were possible to be detected when much harder erodent particles were used in the test. In addition, Stellite-6 should exhibit metal ductility and toughness rather than brittle materials since it is a metal matrixed composite. In contrast, Figure 8a,b show microcracks and deep cavities showing de-bonding due to only brittle erosion on the WC-12Co coating. Deep cavities were clearer on the eroded surface tested at the impingement angle at 90° in Figure 8b than that found at 30° in Figure 8a. The H_p/H_t ratio of WC-12Co coating was 3.33 Hv, the lowest among all samples with the E_{90}/E_{30} ratio exceeding 1 which indicated brittle erosion. The brittle behaviour was also caused by the cermet composite material itself. Porosity was another factor that affected the morphology after erosion testing as well as the H_p/H_t ratio of WC-12Co coating. This resulted in high erosion rates despite the higher hardness than Stellite-6 coatings. The improvement in erosion resistance of Stellite-6 coating was also contributed to by the increase in strength and toughness due to the added cobalt content [19]. Further, the HVOF process' compatibility resulted in the coating's high hardness and low porosity.

4. Conclusions

The HVOF process was used to deposit Stellite-6 and WC-12Co coatings on boiler tube steel, SA213-T22. This resulted in a moderately high hardness, low porosity and a dense coating. Erosion testing was done for uncoated and coated using SiC to clarify erosion rates in a short period of time. The conclusion can be drawn as follows.

1. The erosion of uncoated SA213-T22 steel showed a ductile mode with ploughing and microcutting morphology and SiC embedment on the surface. The erosion rates were lower than the intrinsic value due to the change in surface condition from metal to composite. Thus, evaluation of erosion for materials with extremely low hardness than SiC will result in errors. While in the case of high hardness materials such as Stellite-6 and WC-12Co, SiC embedment did not occur on the surface. This made it possible to apply SiC as an erodent particle for erosion testing.
2. The velocity exponent indicates erosion sensitivity. In the case of uncoated SA213-T22 steel with SiC embedment, the change of velocity exponent from 2.3 to the value exceeding 3 showed the drastic change in the surface condition. While, the Stellite-6 and WC-12Co coatings had values of 2, which correspond to traditional literature [3,27,42].
3. Stellite-6 is a metal matrixed composite, whereas WC-12Co coating is a cermet composite. As a result, erosion will behave differently. In the case of cermet composite, WC-12Co coating showed only brittle erosion. While Stellite-6 showed morphology with some ductile erosion. Thus, its erosion behaviour exhibited brittle dominant erosion.
4. The evaluation results showed better erosion resistance of Stellite-6 than WC-12Co coating. This was contributed to the strength and toughness of the metal matrixed composite structure and the low porosity of the coating. In the case of WC-12Co coating, further optimization may be required to reduce the porosity and brittle phase of W_2C.

Acknowledgments: The authors acknowledge the kind support for materials (SA213–T22 boiler steel) provided by Maemoh Power Plant, Electricity Generating Authority of Thailand (EGAT) and the high velocity oxy-fuel spraying system supported by Hummingbird Corporation Co., Ltd. This research was funded by King Mongkut's University of Technology North Bangkok, Thailand (KMUTNB-FF-65-31).

References

1. Ramesh, M.; Prakash, S.; Nath, S.; Sapra, P.K.; Venkataraman, B. Solid particle erosion of HVOF sprayed WC-Co/NiCrFeSiB coatings. *Wear.* **2010,** 269, 197-205.
2. Sundararajan, G. The solid particle erosion of metallic materials: the rationalization of the influence of material variables. *Wear*. **1995,** 186, 129-144.
3. Sundararajan, G.; Roy, M. Solid particle erosion behaviour of metallic materials at room and elevated temperatures. *Tribol. Int.* **1997,** 30, 339-359.
4. Chawla, V.; Chawla, A.; Puri,D.; Prakash, S.; Gurbuxani, P.G.; Sidhu, B.S. Hot orrosion & erosion problems in coal based power plants in India and possible solutions–a review. *J. Met. Mater. Miner.* **2011,** 10, 367.
5. Levy, A. Erosion and erosion-corrosion of metals. *Corros.* 51 (1995) 872-883.
6. Shipway, P.; Hutchings, I. The role of particle properties in the erosion of brittle materials. *Wear.* **1996,** 193, 105-113.
7. Wichianrat, P.; Dateraksa, K.; Sujirote, K.; Chumphu, A. Wear behaviour of alumina nozzles by sand blasting. *J Metals Mater Miner.* 20 (2010) 15-18.
8. Vite, M.; Laguna, J.; Baldenebro, R.; E.A. Gallardo, E.A.; Vera, E.; Vite, J.; Study of solid particle erosion on AISI 420 stainless steel using angular silicon carbide and steel round grit particles. *Wear.* **2013,** 301, 383-389.
9. Ball, A.; The mechanisms of wear, and the performance of engineering materials, *J. South. Afr. Inst. Min. Metall.* **1986,** 86, 1-13.
10. Wellman, R.; Nicholls, J. High temperature erosion–oxidation mechanisms, maps and models. *Wear.* **2004,** 256, 907-917.
11. Bonu, V.; Barshilia, H.C. High-Temperature Solid Particle Erosion of Aerospace Components: Its Mitigation Using Advanced Nanostructured Coating Technologies. *Coatings.* **2022,** 12, 1979.
12. Mangla, A.; Chawla, V.; Singh, G. Comparative study of hot corrosion behavior of HVOF and plasma sprayed Ni20Cr coating on SA213 (T22) boiler steel in Na_2SO_4-60% V_2O_5 environment. *Int. j. eng. sci. res. technol.* **2017,** 4, 2348-8034.
13. Sapate, S.; Roy, M. Solid particle erosion of thermal sprayed coatings. Thermal Sprayed Coatings and their Tribological Performances. *IGI Global.* **2015,** pp. 193-226.
14. Singh, P.K.; Mishra, S. Erosion performance of detonation gun deposited WC–12Co, Stellite 6 and Stellite 21 coatings on SAE213-T12 steel. *Tribol.—Mater. Surf. Interfaces.* **2020,** 14, 229-239.
15. Kumar, M.; Singh, H.; Singh, N.; Joshi, R.S. Erosion–corrosion behavior of cold-spray nanostructured Ni–20Cr coatings in actual boiler environment. *Wear.* **2015,** 332, 1035-1043.
16. Sidhu, H.S.; Sidhu, B.S.; Prakash, S. Mechanical and microstructural properties of HVOF sprayed WC–Co and Cr_3C_2–NiCr coatings on the boiler tube steels using LPG as the fuel gas. *J. Mater. Process. Technol.* **2006,** 171, 77-82.
17. Kim, H.J.; Hwang, S.Y.; Lee, C.H.; Juvanon, P. Assessment of wear performance of flame sprayed and fused Ni-based coatings. *Surf. Coat. Technol.* **2003,** 172, 262-269.
18. Sharma, A.; Goel, S. Erosion behaviour of WC–10Co–4Cr coating on 23-8-N nitronic steel by HVOF thermal spraying. *Appl. Surf. Sci.* **2016,** 370, 418-426.
19. Sierens, A.; Vanvooren, J.; Deplus, K.; Faes,K.; De Waele, W.; Review on the possible tool materials for friction stir welding of steel plates, *Sustainable Construction and Design.* **2014,** 5.
20. Singh, H.; R. Joshi, Kumar, M.; Singh, N.; Corrigendum to 'Erosion-corrosion behaviour of cold-spray nanostructured Ni–20Cr coatings in actual boiler environment. *Wear.* **2015,** 332–333.
21. Peat, T.; Galloway, A.; Toumpis, A.; McNutt, P.; Iqbal, N.; The erosion performance of particle reinforced metal matrix composite coatings produced by co-deposition cold gas dynamic spraying, Appl. *Surf. Sci.* **2017,** 396, 1623-1634.
22. Hejwowski, T.; Szala, M.; Wear-Fatigue Study of Carbon Steels, Advances in Science and Technology. *Res. J.* **2021,** 15.
23. Weronski, A.; Hejwowski, T.; Effect of stress on abrasive and erosive wear of steels and sprayed coatings, Vacuum, **2008,** 83, 229-233.
24. Suckling, M.; Allen, C. Critical variables in high temperature erosive wear. *Wear.* **1997,** 203, 528-536.
25. Promdirek, P.; Chandra-Ambhom, S.; Prasong, R.; Riittirat, S; Pompaisansakul, N. Influence of gas tungsten arc welding parameters on the high-temperature erosion-corrosion resistance of Incoloy 800 cladded by Stellite 12 for the application as thermowell. *Mater. Sci. Forum.* **2011,** 248-253.

26. Promdirek, P.; Chandra-Ambhom, S.; Tongtae, C.; Anantawirun, C; Buaphuen, C. Characterization and Failure Analysis of Incoloy 800 Used as Thermowell Subjected to High Temperature Erosion-Corrosion. *Mater. Sci. Forum.* **2008,** 673-680.
27. Finnie, I. Erosion of surfaces by solid particles. *Wear.* **1960,** 3, 87-103.
28. Liu, Z.; Wan, S.; Nguyen, V.; Zhang, Y. A numerical study on the effect of particle shape on the erosion of ductile materials. *Wear.* **2014,** 313, 135-142.
29. Tabakoff, W.; Shanov, V.; Erosion rate testing at high temperature for turbomachinery use. *Surf. Coat. Technol.* **1995**, 76, 75-80.
30. Berget, J. Influence of powder and spray parameters on erosion and corrosion properties of HVOF sprayed WC-Co-Cr coatings. **1998.**
31. Yuan, J.; Zhan, Q.; Huang, J.;Ding, S.; Li, H. Decarburization mechanisms of WC–Co during thermal spraying: Insights from controlled carbon loss and microstructure characterization. *Mater. Chem. Phys.* **2013,** 142, 165-171.
32. Ding, X.; Ke, D., Yuan, C.; Ding, Z.; Cheng, X. Microstructure and cavitation erosion resistance of HVOF deposited WC-Co coatings with different sized WC. *Coatings.* **2018,** 8, 307.
33. Kreye, H. Characteristics of coatings produced by high velocity flame spraying. *Thermal Spraying.* **1989,** 2, 24.
34. Mirshekari, G.; Daee, S.; Bonabi, S.F.; Tavakoli, M.; Shafyei, A.;Safaei, M. Effect of interlayers on the microstructure and wear resistance of Stellite 6 coatings deposited on AISI 420 stainless steel by GTAW technique. *Surf. Interfaces.* **2017,** 9, 79-92.
35. Stack, M.; Mathew, M. Transitions in microabrasion mechanisms for WC-Co (HVOF) coated steel, Proceedings of the Institution of Mechanical Engineers. *Part J: Journal of Engineering Tribology.* **2005,** 219, 49-57.
36. Jonda, E.; Szala, M.; Sroka, M.; Łatka, L.; Walczak, M.; Investigations of cavitation erosion and wear resistance of cermet coatings manufactured by HVOF spraying, *Appl. Surf. Sci.* **2023,** 608, 155071.
37. Jonda, E.; Latka, L.; Comparative analysis of mechanical properties of WC-based cermet Coatings sprayed by HVOF onto AZ31 magnesium alloy substrates, Advances in Science and Technology. *Res. J.*, **2021,** 15.
38. Roy, M.; Ray,K.; Sundararajan, G.; An analysis of the transition from metal erosion to oxide erosion, *Wear.* **1998,** 217, 312-320.
39. Kumar, K.; Kumar, S.; Singh, G.; Singh, J.P.; Singh, J. Erosion wear investigation of HVOF sprayed WC-10Co4Cr coating on slurry pipeline materials. *Coatings.* **2017,** 7, 54.
40. Arabnejad, H.; Mansouri, A.; Shirazi, S.; McLaury, B.; Evaluation of solid particle erosion equations and models for oil and gas industry applications. SPE Annual Technical Conference and Exhibition. *Soc. Pet. Eng. J.* **2015.**
41. ASTM G76-05. Standard practice for conducting erosion tests by solid particle impingement using gas jets. *ASTM International West Conshohocken.* **1983**.
42. Basu, P; Kefa, C; Jestin L. Boilers and burners: design and theory, *Springer Science & Business Media.* **2012.**
43. Sapate, S.; RamaRao, A. Effect of erodent particle hardness on velocity exponent in erosion of steels and cast irons. *Mater. Manuf. Process.* **2003,** 18, 783-802.
44. Keshavamurthy, R.; Naveena, B.; Sekhar, N. Thermal spray coatings for erosion-corrosion protection. Production, properties, and applications of high temperature coatings. *IGI Global.* **2018,** 246-267.
45. Heath, G.; Stack, M.; Rehberg, M.; Kammer,P.; The erosion of functionally graded coatings under fluidized bed conditions, **1995.**